General Disclaimer

One or more of the Following Statements may affect this Document

- This document has been reproduced from the best copy furnished by the organizational source. It is being released in the interest of making available as much information as possible.

- This document may contain data, which exceeds the sheet parameters. It was furnished in this condition by the organizational source and is the best copy available.

- This document may contain tone-on-tone or color graphs, charts and/or pictures, which have been reproduced in black and white.

- This document is paginated as submitted by the original source.

- Portions of this document are not fully legible due to the historical nature of some of the material. However, it is the best reproduction available from the original submission.

NASA TECHNICAL MEMORANDUM

NASA TM X-71707

NASA TM X-71707

OUTDOOR FLAT-PLATE COLLECTOR PERFORMANCE PREDICTION FROM SOLAR SIMULATOR TEST DATA

by Frederick F. Simon and Edgar H. Buyco
Lewis Research Center
Cleveland, Ohio 44135

TECHNICAL PAPER to be presented at 10th Thermal Physics Conference sponsored by the American Institute of Aeronautics and Astronautics
Denver, Colorado, May 27-29, 1975

OUTDOOR FLAT-PLATE COLLECTOR PERFORMANCE PREDICTION FROM SOLAR SIMULATOR TEST DATA

Frederick F. Simon and Edgar H. Buyco
National Aeronautics and Space Administration
Lewis Research Center
Cleveland, Ohio

ABSTRACT

This paper describes how collector performance obtained from test data with a simulator can be modified for real-life conditions. The approach taken is to correct the performance data obtained with the simulator for the variable conditions of ambient temperature, wind, incident angle, flow rate, etc., that are encountered in outdoor conditions. Modification of simulator data is accomplished by combining experiment with theory. The technique is demonstrated by application to a spectrally selective and a nonselective type of collector. This kind of modified simulator collector performance data should be valuable in solar systems analyses and for collector performance ranking based on all-day calculated conditions.

INTRODUCTION

An area presently being investigated by the NASA-LeRC in its efforts to aid in the utilization of alternate energy sources is the use of solar energy for the heating and cooling of buildings. An important part of this effort is the investigation of flat-plate collectors which have the potential to be efficient, economical, and reliable. Efficient collectors will be an important consideration in the realization of effective solar cooling systems. The approach being taken at the Lewis Research Center for determining collector performance is to test collectors under simulated (indoor) and actual (outdoor) conditions.

Indoor testing of coolectors with a solar simulator has permitted ranking of collectors on the basis of performance[1] and a determination of the key parameters affecting collector performance[2]. The solar simulator approach has been extremely effective in evaluating collector performance on a relative basis. The questions which need answering are: (1) How good are the simulator results when compared to actual conditions? (2) Since the performance data is determined under standard conditions of wind, ambient temperature and flow rate, what corrections are needed for actual conditions other than the standard?

If it can be shown that the simulator does indeed do a good job of simulating actual conditions and that the simulator results can be corrected for conditions other than those of the simulator tests, then the simulator results can be used in the design and analysis of solar heating and cooling systems. The application of simulator data to outdoor conditions would also permit performance ranking to be based on all-day performance calculations. The objective of this paper is to present evidence of the simulation ability of the indoor collector test approach, and to demonstrate how collector performance from the simulator can be modified to account for variable outdoor conditions.

SOLAR SIMULATOR

Experimental Facility

A drawing of the facility is presented in Fig. 1. The primary components of the facility are the energy source (solar simulator), the liquid flow loop, and the instrumentation and data acquisition equipment. A summary of information describing the facility is presented in Table 1. More detail on the manner of testing, instrumentation, etc., may be found in Refs. 1, 2 and 3.

Solar Simulator

The basic rational for the use of a solar simulator for the testing of solar collectors was given in Ref. 4. This approach allows for controlled conditions that make it possible to properly compare the performance of different collector types. The simulator shown in Fig. 1 consists of 143 tungsten-halogen 300-watt lamps placed in a modular array with Fresnel lenses placed at the focal distance so as to collimate the radiation.

A comparison of spectral characteristics of the simulator output with air mass-2 sunlight is given in Table II. Table II demonstrates that the solar simulator does an excellent job of simulating the sun's radiation in this application. The fact that the spectral qualities of the simulator come close to actual sunshine is a key requirement in using the indoor approach to simulate actual conditions. For more detail information on the spectral qualities of the simulator and other information see Ref. 3.

Correlative Method

The experimental efficiency calculated by the use of

$$\eta = GC_p(T_o - T_i)/q_{DR} \tag{1}$$

is calculated in a manner corresponding to the following basic collector equations.

$$\eta = \alpha\tau - U_L(\overline{T}_p - T_a)/q_{DR} \tag{2}$$

$$\eta = F'[\alpha\tau - U_L(\overline{T}_f - T_a)/q_{DR}] \tag{3}$$

$$\eta = F_R[\alpha\tau - U_L(T_i - T_a)/q_{DR}] \tag{4}$$

Examples of how these equations can be used in conjunction with the experimental data were given in Refs. 1, 2 and 4. The performance curves from Ref. 2 for a black-nickel two-glass collector and a black paint two-glass collector are given in Figs. 2(a) to (c) and 3(a) to (c), respectively. We see from Eqs. (2-4) and Figs. 2 and 3 that depending on how we plot the basic performance we can

obtain information on the basic parameters affecting collector performance ($\alpha\tau$, F', F_R and U_L) and have an approach by which to obtain basic correlating equations. The correlating equations for the data of Figs. 2 and 3 have the basic form of

$$\eta = a_\phi - b_\phi\phi - C_\phi\phi^2 \quad (5)$$

$$\eta = a_\psi - b_\psi\psi - C_\psi\psi^2 \quad (6)$$

$$\eta = a_\theta - b_\theta\theta - C_\theta\theta^2 \quad (7)$$

where

$$\phi = (\overline{T}_p - T_a)/q_{DR}$$

$$\psi = (\overline{T}_f - T_a)/q_{DR}$$

and

$$\theta = (T_1 - T_a)/q_{DR}$$

Comparing Eqs. (5-7) with the corresponding Eqs. (2, 3 and 4), we see the following relationships:

$$(\alpha\tau)_s = a_\phi \quad (8)$$

$$(F'\alpha\tau)_s = a_\psi \quad (9)$$

$$(F_R\alpha\tau)_s = a_\theta \quad (10)$$

$$U_{Ls} = b_\phi + C_\phi\phi \quad (11)$$

$$(F'U_L)_s = b_\psi + C_\psi\psi \quad (12)$$

$$(F_RU_L)_s = b_\theta + C_\theta\theta \quad (13)$$

These relationships will form the basis later for modifying the basic correlation Eqs. (5-7) to environmental conditions other than those used in obtaining these equations (conditions of Table I).

Another check of the simulator's spectrum as compared to that of the sun's is to calculate the experimental value of absorptivity for a wavelength sensitive surface such as black nickel. Using Eq. (8) and the measured value of glass transmittance, we can calculate the value of the absorptivity determined with the simulator and compare it with the value obtained with a spectrophotometer. The comparison shown in Table III gives further evidence of the simulator's ability to simulate the spectrum of the sun.

Indoor vs. Outdoor Data

Collectors of the same type and design as those of Figs. 2 and 3 were tested under contract to NASA-LeRC by the Honeywell Corporation in Minneapolis, Minnesota. A black-nickel two-glass and a black-paint two-glass collectors were tested both indoors under simulated conditions and outdoors. The solar simulator used by Honeywell is a copy of the NASA-LeRC solar simulator. The results of the indoor tests with the two collector types were used to predict the outdoor tests of these same collectors. A comparison of the indoor and outdoor tests is given in Fig. 4. The time previous to the steady state arrow of 180° F shown in Fig. 4 was a period in which the collector and the rest of the system was warming up. This period can be considered a total test system transient. This period, as shown in Fig. 4, existed for about 1 hour. Another collector transient period occurred from 12 p.m. to 1 p.m. due to a condition in which the incident flux decreased. The use of the steady state simulator results are not expected to be completely applicable during a transient period due to the collector heat capacity. The effect of this is a lag between the calculated and experimental energy collected (useful solar flux, q_u). This paper does not consider transient effects. However, for collectors of small heat capacity these transient effects will have little effect on all day collector performance. This transient effect needs to be considered in the dynamic analysis of solar systems. It appears from Fig. 4 that the steady-state collector results obtained with the solar simulator does a good job of predicting the steady-state outdoor tests.

Method Of Modifying Simulator Data

The first step in establishing modified versions of the simulator data is to rework the correlation Eqs. (5-7) into a modified form. The three parameters requiring modification so that variable conditions may be comprehended are the flow factor (F_R), the overall heat loss coefficient (U_L) and the product of transmittance and absorptance ($\alpha\tau$). Correction factors related to the simulator values of F_R, U_L and $\alpha\tau$ are as follows:

$$K_{FR} = F_R/F_{Rs} \quad (14)$$

$$K_{U_L} = U_L/U_{Ls} \quad (15)$$

$$K_{\alpha\tau} = \alpha\tau/(\alpha\tau)_s \quad (16)$$

Combining Eqs. (14-16) with Eqs. (10,13 and 7) results in a modified version that can be utilized for performance predictions for the direct component of solar energy.

$$\eta = K_{FR}[K_{\alpha\tau}\, a_\theta - K_{U_L}(b_\theta\theta + C_\theta\theta^2)] \quad (17)$$

The method of determining the correction factors (K_{U_L}, K_{FR} and $K_{\alpha\tau}$) follows.

Heat Loss Modification (K_{U_L})

Use of theory leads to an approach for modifying the overall heat loss coefficient (U_L) determined experimentally in the simulator facility. The overall heat loss coefficient has three components as represented by the following equation

$$U_L = U_{L,c} + U_{L,R} + U_{L,e}A_p/A_c \quad (18)$$

The rear conduction loss coefficient ($U_{L,R}$) is easily calculated by

$$k_i/\delta \quad (19)$$

and for the edge loss coefficient the value given by Whillier[5] is appropriate.

$$U_{L,e} = 0.08 \quad (20)$$

For the cover heat loss coefficient ($U_{L,c}$) a solution of the following equation is necessary

Absorber Plate To 1st Cover

$$q_{L,c} = C\left(\overline{T}_p - \overline{T}_{g_1}\right)^n + \frac{\sigma}{(1/\varepsilon_p) + (1/\varepsilon_g)-1}\left(\overline{T}_p^4 - \overline{T}_{g_1}^4\right) \quad (21)$$

1st Cover To 2nd Cover

$$q_{L,c} = C\left(\overline{T}_{g_1} - \overline{T}_{g_2}\right)^n \frac{\sigma}{(2/\varepsilon_g) - 1}\left(T_{g_1}^4 - T_{g_2}^4\right) \quad (22)$$

2nd Cover To Environment

$$q_{L,c} = h_o\left(\overline{T}_{g_2} - T_a\right) + \varepsilon_g \sigma\left(\overline{T}_{g_2}^4 - T_{sky}^4\right) \quad (23)$$

$$U_{L,c} = q_{L,c}/(\overline{T}_p - T_a) \quad (24)$$

The only additional information required for the solution of Eqs. (18-24) is knowledge of the coefficients (C and n) related to convective heat loss. For obtaining this information the equations relating the heat transfer by natural convection are applicable. The following is a summary of possible candidates for predicting heat loss due to natural convection.

De Graaf and Van Der Held[6] made a systematic experimental investigation of heat transfer in enclosed plane air layers in horizontal, oblique and vertical positions. The following equations were deduced

For $\theta_T = 0^o$:

$$Nu_L = 1 \qquad Gr_L < 2\times10^3 \quad (25)$$

$$Nu_L = 0.0507\ Gr_L^{0.40} \qquad 2\times10^3 < Gr_L < 5\times10^4 \quad (26)$$

$$Nu_L = 3.8 \qquad 5\times10^4 < Gr_L < 2\times10^5 \quad (27)$$

$$Nu_L = 0.0426\ Gr_L^{0.37} \qquad Gr_L < 2\times10^5 \quad (28)$$

For $\theta_T = 20^o$:

$$Nu_L = 1 \qquad Gr_L < 2\times10^3 \quad (29)$$

$$Nu_L = 0.0507\ Gr^{0.4} \qquad 2\times10^3 < Gr_L < 3\times10^4 \quad (30)$$

$$Nu_L = 3.6 \qquad 4\times10^4 < Gr_L < 5\times10^5 \quad (31)$$

$$Nu_L = 0.0402\ Gr_L^{0.37} \qquad Gr_L > 2\times10^5 \quad (32)$$

For $\theta_T = 30^o$:

$$Nu_L = 1 \qquad Gr_L < 3\times10^3 \quad (33)$$

$$Nu_L = 0.0588\ Gr^{0.37} \qquad 3\times10^3 < Gr_L < 5\times10^4 \quad (34)$$

$$Nu_L = 0.039\ Gr^{0.37} \qquad Gr_L > 2\times10^5 \quad (35)$$

For $\theta_T = 45^o$:

$$Nu_L = 1 \qquad Gr_L < 4\times10^3 \quad (36)$$

$$Nu_L = 0.0503\ GR_L^{0.37} \qquad 4\times10^3 < Gr_L < 5\times10^4 \quad (37)$$

$$Nu_L = 0.0372\ Gr_L^{0.37} \qquad Gr_L > 2\times10^5 \quad (38)$$

For $\theta_T = 60^o$:

$$Nu_L = 1 \qquad Gr_L < 5\times10^3 \quad (39)$$

$$Nu_L = 0.0431\ Gr^{0.37} \qquad 5\times10^3 < Gr_L < 5\times10^4 \quad (40)$$

$$Nu_L = 0.0354\ Gr^{0.37} \qquad Gr_L > 2\times10^5 \quad (41)$$

For $\theta_T = 70^o$:

$$Nu_L = 1 \qquad Gr_L < 6\times10^3 \quad (42)$$

$$Nu_L = 0.0384\ Gr_L^{0.37} \qquad 10^4 < Gr_L < 8\times10^4 \quad (43)$$

$$Nu_L = 0.0342\ Gr_L^{0.37} \qquad Gr_L > 2\times10^5 \quad (44)$$

For $\theta_T = 90^o$:

$$Nu_L = 1 \qquad Gr_L < 7\times10^3 \quad (45)$$

$$Nu_L = 0.0384\ Gr_L^{0.37} \qquad 10^4 < Gr_L < 8\times10^4 \quad (46)$$

$$Nu_L = 0.0317\ Gr_L^{0.37} \qquad Gr_L > 2\times10^5 \quad (47)$$

De Graaf and Van Der Held concluded from their results that the Nu_L depends only on inclination when the air motion is turbulent and one may freely interpolate between horizontal and vertical positions only if $Gr_L > 10^5$. Between 20^o and 70^o interpolation can be made if $5\times10^3 < Gr_L < 6\times10^4$.

Tabor[7] recommended the results of his correlation using the 1954 Housing and Home Finance Agency Report 32 which in dimensionless form may be written in generalized form as

For $\theta_T = 0^o$:

$$Nu_L = 0.152\ Gr_L^{0.281} \qquad 10^4 < Gr_L < 10^7 \qquad (48)$$

For $\theta_T = 45^o$:

$$Nu_L = 0.0925\ Gr_L^{0.310} \qquad 10^4 < Gr_L < 10^7 \qquad (49)$$

For $\theta_T = 90^o$:

$$Nu_L = 0.0326\ Gr_L^{0.381} \qquad 1.5x10^4 < Gr_L < 1.5x10^5 \qquad (50)$$

$$Nu_L = 0.0616\ Gr_L^{0.327} \qquad 1.5x10^7 < Gr_L < 10^7 \qquad (51)$$

A subsequent experimental work using fluids whose Prandtl number varied over a very wider range of values was the work of Dropkin and Somercales[8]

For $\theta_T = 0^o$: $Nu_L = 0.069\ Ra_L^{1/3}\ Pr^{0.074}$

$$1.5x10^5 < Ra_L < 7.5x10^8 \qquad (52)$$

For $\theta_T = 30^o$: $Nu_L = 0.065\ Ra_L^{1/3}\ Pr^{0.074}$

$$1.5x10^5 < Ra_L < 7.5x10^8 \qquad (53)$$

For $\theta_T = 45^o$: $Nu_L\ 0.059\ Ra_L^{1/3}\ Pr^{0.074}$

$$1.5x10^5 < Ra_L < 2.5x10^8 \qquad (54)$$

For $\theta_T = 60^o$: $Nu_L = 0.057\ Ra_L^{1/3}\ Pr^{0.074}$

$$1.5x10^5 < Ra_L < 2x5x10^8 \qquad (55)$$

For $\theta_T = 90^o$: $Nu_L = 0.049\ Ra_L^{1/3}\ Pr^{0.074}$

$$5x10^4 < Ra_L < 2.5x10^8 \qquad (56)$$

The above equations may put into a form first used by Hottel and Woertz[9].

$$q = C(T - T_g)^n \qquad (57)$$

The constant C in Eq. (57) is a function of temperature and angle of tilt and the value of n depends on whether the fluid between the walls is in laminar or turbulent condition. Using the above equations for natural convection heat loss, values of C and n were caluclated for a black-nickel two-glass and a black paint two-glass collector, both of which had a gap distance for free convection of 1 1/4 in. The results of these calculations are shown in Table IV. Also shown in Table IV are the values of C and n suggested by Whillier[5]. Use of Table IV with Eqs. (21-24) results in theoretical vlaues of the cover heat loss coefficient ($U_{L,C}$) which can be compared to the simulator determined heat loss coefficients. The simulator cover heat loss coefficient was determined with Eqs. (18-20) by using the values of the experimental overall heat loss coefficient and the collector back and edge loss coefficient. The experimental overall heat loss coefficient was calculated using Eq. (11) with on average flux of 250 BTu/hr ft^2. The edge and rear collector losses were approximately 15% of the total loss in the case of the black paint two-glass collector and 21% for the black nickel two-glass collector. The comparison between the theoretical and experimental cover heat loss coefficients are shown in Fig. 5. Figure 5 appears to indicate that the experimental heat loss is larger than predicted from theory. The difference between theory and experiment is especially dramatic in the case of the selective black nickel collector where the majority of the heat loss is by free convection.

It appears that the convection loss equation suggested by Whillier comes closest to the experimental findings. However, the exponent (n) suggested by Whillier does not satisfy the turbulent conditions (as indicated by Gr) encountered in the two collectors tested. Duffie and Beckman[10] recommend the Home Finance equations. Since these equations do about as well as Whillier's and have an exponent (n) consistent with the Gr no, they will be used for modification of the experimental values of heat loss. Simply, the values of C in the Home Finance equation are corrected so that the theoretical value of the cover heat loss coefficient (U_{Lc}) is equal to the experimental value of the cover heat loss coefficient. Using these "experimental" values of C in Eqs. (21-24), we have a means by which we can calculate the effect of ambient temperature (fig. 6), sky temperature (fig. 7(a) and 7(b) and wind (fig. 8). Figure 6 shows that the effect of ambient temperature on the heat loss coefficient is most pronounced at the lower plate temperatures for the black-nickel two-glass collector. This effect could be explained by the low radiation heat loss component of the black nickel collector causing a cooler glass condition. A glass temperature which is lower than one would get at high plate temperature or high plate emissivity increases the convection losses and thus increasing the heat loss coefficient. Increased convection losses at lower plate temperatures is a possible explanation of the curve forms shown in Fig. 7. It can be seen from Fig. 8 that the effect of wind on the heat loss coefficient is to increase it, as expected, but for wind speeds greater than the simulator wind speed, the increase in heat loss due to wind speed is small.

In general, once we have fixed on a value of C using the experimental data we can caluclate the cover heat loss coefficient at different conditions.

$$U_{L,c} = f(T_a, T_{sky}, h_o, \theta_T, T_p) \qquad (58)$$

Use of Eqs. (18-20) permits a calculation of the overall heat loss coefficient:

$$U_L = f(T_a, T_{sky}, h_o, \theta_T, T_p) \qquad (59)$$

The simulator results may be expressed:

$$U_{L,s} = f(T_a = \text{const.}, = T_{sky},$$

$$h_o = \text{const.}, \theta_T = \text{const.}, T_p) \qquad (60)$$

The heat loss modifying factor (Eq. (15)) is obtained from Eqs. (59) and (60).

Since the simulator results are obtained at a fixed tilt angle, a way is needed to modify the experimental value of C. The present collector experiments were run at a tilt angle of 57°.

Using the variation of c with respect to tilt angle according to the equation for DeGraaf and Van Der Held we have:

$$C_{\theta_T} = -k\ 6.38\times10^{-4}\ (\theta_T - 57) + C_{\theta_T=57}(\text{exp}) \qquad (61)$$

where

$$k = C_{\theta_T=57}(\text{exp})/C_{\theta_T=57}(\text{theory}) \qquad (62)$$

Figure 9 shows the effect of tilt angle by utilizing Eq. (61) with the basic theoretical equations. Figure 9 suggests that tilt angle has a 10-20% effect over the entire range of tilt range or about a 1-2% per tilt angle degrees.

Incident Angle Modification ($K_{\alpha\tau}$)

The modification for the variation of the product of absorptance and transmittance ($\alpha\tau$) may be obtained from curves of transmittance and absorptance versus incident angle. To determine the modifying factor ($K_{\alpha\tau}$) one simply uses the following relationship:

$$K_{\alpha\tau} = (\alpha\tau)_{\theta_i}/(\alpha\tau)_{\theta_i=0} = (\alpha\tau)_{\theta_j}/(\alpha\tau)_s \qquad (63)$$

Equation (63) is an incident angle modifier for the simulator results obtained at zero incident angle. Calculated results of this modifier for the black-nickel two-glass and black-paint two-glass collector are shown in Fig. 10. The calculations of Fig. 10 are based on theoretical transmission curves for glass and the reflectivity measurements for a non-selective black paint and a selective black nickel coating.

A correlation for the product of $\alpha\tau$ was suggested by Souka and Safruat[12]. This correlation has the following general form

$$\alpha\tau = a - b/\cos\theta_i;\ \theta_i < \pi/2 \qquad (64)$$

Use of Eq. (64) allows the following expression for the incident angle modifier.

$$K_{\alpha\tau} = 1.0 - b_o(1/\cos\theta_i - 1) \qquad (65)$$

The results of Fig. 10 for the black paint two-glass collector are plotted in the manner of Eq. (65) in Fig. 11. For the range of incident angles of interest in determining collector performance, Fig. 11 demonstrates the validity of Eq. (65). The constant (b_o) of Eq. (65) should be a function of the number of collector covers, the absorber surface and the internal physical structure of the collector.

Another way to determine the incident angle modifying factor is to use the Lewis simulator facility, since this facility permits a determination of collector performance at different incident angles. The approach is to determine collector performance at an inlet temperature (T_i) equal to the ambient temperature (T_a). According to Eq. (4) the effect of this procedure is to relate the collector efficiency to the product of the absorptance and transmittance.

$$\eta = F_R\alpha\tau \qquad (66)$$

By performing the above procedure at different incident angles and realizing that the flow factor (F_R) is independent of incident angle, one is able to determine the incident angle modifier according to Eq. (63). Examples of the results of this procedure for two selective surfaces are given in Fig. 11. The experimental points in Fig. 11 for the two selectively coated collectors tested appear to follow the calculated line for the black-paint two-glass collector.

Flow Factor Modifier (K_{FR})

To assess the effect of flow rate on performance, the equation derived by Whillier[5] is applicable.

$$F_R = F'\ (GC_p)/(F'U_L)\left(1 - e^{-F'U_L/GC_p}\right) \qquad (67)$$

Where the plate efficiency factor for the type of collectors being used as examples in this paper can be represented by

$$F' = 1\Big/\left(\frac{aU_L}{h_f} + b\right) \qquad (68)$$

Since the value of b is essentially equal to one, the plate efficiency factor determined from the simulator results (F'_s) can be corrected for different flow rates and heat loss as follows:

$$F' = F'_s\ H/H_s \qquad (69)$$

where

$$H = 1\Big/\left(\frac{aU_L}{h_f}\right) + 1$$

and a is determined from the simulator values of F', U_L and h_f. The collectors of this paper have a value of the plate efficiency factor of 0.97 for the conditions stated in Figs. 2 and 3[2]. For these collectors Eq. (69) would be

$$F' = 0.97\ H/H_s \qquad (70)$$

Use of Eq. (67) allows a calculation of the flow factor as follows:

$$K_{FR} = \frac{F_R}{F_{Rs}} = \frac{B}{B_s}\left(\frac{F'}{F'_s}\right)\frac{(1 - e^{-B})}{(1 - e^{-B_s})} \qquad (71)$$

where

$$B = GC_p / F'U_L \qquad (72)$$

Equations (70) and (71) become the basis by which a flow factor may be calculated when the following conditions differ from the conditions of the simulator collector tests:

1. Flow Rate - G
2. Heat Loss - U_L
3. Type of Heat transfer fluid - C_p, h_f

Diffuse and Direct Energy Modifiers K_{Df}, K_{DR}

The collection performance equation, Eq. (17), is only valid for the direct component of solar energy since the solar simulator output gives an essentially direct radiation flux. Equation (17) needs to be modified to include diffuse radiation. For the case of diffuse and direct radiation in the plane of the collector, the basic equation (Eq. 4) can be written as follows:

$$\eta = F_R\left[\frac{\alpha\tau q_{DR}}{q_T} + \frac{\overline{\alpha\tau} q_{DF}}{q_T} - \frac{U_L(T_1 - T_a)}{q_T}\right] \qquad (72)$$

Defining:

$$K_{DR} = q_{DR}/q_T$$

and

$$K_{DF} = q_{DF}/q_T$$

and comparing Eq. (72) with Eq. (17) we obtain:

$$\eta = K_{FR}\left[K_{\alpha\tau}K_{DR}a_\theta + K_{DF}\,\overline{\alpha\tau} - K_{U_L}(b_\theta\theta + C_\theta\theta)\right] \qquad (73)$$

with

$$\theta = (T_1 - T_a)/q_T$$

Equation (73) is the collector efficiency equation which can be utilized for outdoor performance prediction. A sample calculation is made to demonstrate the use of Eq. (73).

Sample Calculation

Basic solar and weather information (θ_i, T_a, wind, q_{DF}, q_{DR}, q_T) is the input needed to modify the simulator data for outdoor conditions.

For the purpose of a sample calculation the Blue Hill, Mass. solar data of Dec. 20, 1955, is used. It is assumed that the wind speed was the same as in the simulator facility (7 mi/hr). The effective sky temperature for radiation is calculated with the following equation of Ward(11).

$$T_{sky} = 0.914\ T_a \quad \text{(Absolute temp.)} \qquad (74)$$

The collector tilt angle is 65.0° and the flow rate the same as employed in the tests with the simulator facility (10 lb/hr ft^2). Using the methods described above a determination is made of the heat loss modifier (K_{U_L}), incident angle modifier ($K_{\alpha\tau}$, fig. 10), diffuse energy modifier (K_{DF}) and the direct energy modifier (K_{DR}). Table V lists these modifiers and the required collector performance constants obtained from the simulator tests. The value of $\overline{\alpha\tau}$ for the use in Eq. (72) can be determined from the following equation derived in Appendix A

$$\overline{\alpha\tau} = \alpha\tau_{\theta_i=0}\ K_{\alpha\tau,\theta_i=60^\circ} \qquad (75)$$

Table V shows that the results for heating ($T_1 = 120^\circ$ F) for the day chosen gives all-day efficiencies of 39.7% and 32.5% for the black-nickel two-glass and balck-paint two-glass collectors, respectively. The heat loss modifier for the black-nickel collector was significantly larger than for the black-paint collector. One possible reason for this difference is the lower glass temperatures for the black-nickel collector due to a smaller radiation component. A lower glass temperature will increase convection losses. This effect can better be seen in Figs. 6 and 7 where a condition of low-plate temperature or low-plate emissivity (black-nickel collector) gives a higher differential of the heat loss coefficient between the calculated value and the simulator test value. When the radiation component becomes significant (high T_p) the effect of ambient temperature and sky temperature on the heat loss modifier becomes smaller.

One factor which the performance calculations do not at present consider is the effect of aging and the effect of dust, etc., on collector performance. It should be possible to experimentally determine modifiers that will correct for such an effect. These experimentally determined modifiers can be incorporated into Eq. (72).

CONCLUSION

A method is presented for the modification of solar simulator results for conditions encountered outdoors. The modified performance equation is:

$$\eta = K_{FR}[K_{\alpha\tau}K_{DR}a_\theta + K_{DF}\overline{\alpha\tau} - K_{U_L}(b_\theta\theta + C_\theta\theta^2)]$$

Where a_θ, b_θ and C_θ are constants determined in the solar simulator facility, and the other factors are used to modify flow rate and fluid type (K_{FR}), incident angle ($K_{\alpha\tau}$), direct solar energy (K_{DR}) diffuse solar energy (K_{DF}) and heat loss (K_{U_L}).

Use of the above equation permits a means by which collector tests performed under controlled indoor conditions can be used for collector steady-state performance evaluation under outdoor conditions.

APPENDIX A

Determination Of Product Of Absorptivity And Transmittance For Diffuse Radiation ($\overline{\alpha\tau}$)

The product of absorptivity and transmittance for diffuse radiation can be shown to be expressed as follows:

$$\overline{\alpha\tau} = 2 \int_0^{\pi/2} \alpha\tau \sin\theta_i \, d\theta_i \qquad (A\text{-}1)$$

From Eq. (65) the following is obtained

$$\alpha\tau = (\alpha\tau)_{\theta_i=0} \left[1.0 - b_o \left(\frac{1}{\cos\theta_i} - 1.0\right)\right] \qquad (A\text{-}2)$$

Combining Eqs. (A-1) and (A-2) and integrating results in

$$\overline{\alpha\tau} = \alpha\tau_{\theta_i=0}[1 - b_o] \qquad (A\text{-}3)$$

Comparing Eq. (A-3) with Eq. (65) results in the following identity

$$K_{\overline{\alpha\tau}} = \frac{\overline{\alpha\tau}}{\alpha\tau_{\theta_i=0}} = K_{\alpha\tau_{\theta_i=60^o}} \qquad (A\text{-}4)$$

Therefore the product of absorptivity and transmittance for diffuse radiation ($\overline{\alpha\tau}$) may be determined as follows:

$$\overline{\alpha\tau} = \alpha\tau_{\theta_i=0} \left(K_{\alpha\tau_{\theta_i=60^o}}\right) \qquad (A\text{-}5)$$

SYMBOLS

A_c	collector area, ft^2
A_p	area associated with collector perimeter, ft^2
C	constant
C_p	heat capacity, BTu/lbm ^oF
F_R	collector flow efficiency factor, dimensionless
F'	collector plate efficiency factor, dimensionless
g	acceleration due to gravity, 32.17 ft/sec^2
Gr_L	grashot number based on L_ε, dimensionless
G	flow per unit of absorber area lb/hr ft^2
ho	wind coefficient BTu/hr ft^2 ^oF
h_f	heat transfer coefficient BTu/hr ft^2 ^oF
k	thermal conductivity BTu/hr ft ^oF
L	distance between cover plates, ft
m,n	exponents, dimensionless
Nu_L	Nusselt number based in L, dimensionless
Pr	Prandtl number, dimensionless
q	energy flux, BTu/hr ft^2
q_L	energy loss, BTu/hr ft^2
Ra_L	Ragleigh number based on L, dimensionless
T	temperature ^oR
T_o	outlet temperature, ^oF
T_1	inlet temperature ^oF
U_L	overall heat loss coefficient, BTu/hr ft ^oF
α	coating absorptivity, dimensionless
$\overline{\alpha\tau}$	absorptivity transmittance product for diffuse radiation
δ	insulation thickness, in.
ε	emissivity of coating
η	collector efficiency, dimensionless
θ_i	incident angle of radiation
θ_T	collector tilt angle
σ	Stefan-Boltzmann constant, BTu/hr ft^2 $^oR^4$
τ	transmittance

Subscripts

a	ambient
c	cover
DF	diffuse in the plane of the collector
DR	direct in the plane of the collector
e	edge
f	fluid
g_1	inner glass
g_2	outer glass
L	based on thickness of gas layer
i	insulation
p	plate
R	rear
s	simulator
T	total
u	useful

Superscripts

—	average

REFERENCES

1. Simon, F. F., "Status of the NASA-Lewis Flat-Plate Collector Tests with a Solar Simulator," presented at NSF/RANN Workshop on Solar Collectors for Heating and Cooling of Buildings, New York, N.Y., Nov. 1974.
2. Simon, Frederick F.: Comparison Under a Simulated Sun of Two Black-Nickel-Coated Flat-Plate Solar Collectors with a Nonselective-Black-Paint-Coated Collector. NASA TM X-3226, 1975.
3. Yass, K. and Curtis, H. B., "Low-Cost, Air Mass 2 Solar Simulator," TM X-3059, 1973, NASA.
4. Simon, F. F. and Harlamert, P., "Flat-Plate Collector Performance Evaluation. The Case for a Solar Simulation Approach," presented at International Solar Energy Society, Cleveland, Oh., Oct. 3-4, 1973.
5. Whillier, A., "Design Factors Influencing Solar Collector Performance," in American Society Heating, Refrigeration and Air Conditioning Engineers, Technical Committee on Solar Energy Utilization, 1967, pp. 27-40.

6. DeGraaf, J. G. A. and Van Der Held, E. F. M., "Correlation Between the Heat Transfer and the Convection Phenomena in Enclosed Plane Air Layers," Appl. Sci. Res., Vol. A3, 1953, pp. 393-409.

7. Tabor, H., "Radiation Convection and Conduction Coefficients in Solar Collectors," Res. Council Israel Bull., Vol. 6C, No. 3, Aug. 1958, pp. 155-176.

8. Dropkin, D. and Somerscales, E., "Heat Transfer by Natural Convection in Liquids Confined by Two Parallel Plates Which are Inclined at Various Angles with Respect to Horizontal," J. Heat Transfer, ASME, Trans. Vol. 87, Feb. 1965, pp. 77-84.

9. Hottel, H. C. and Woertz, B. B., "The Performance of Flat-Plate Solar Heat Collectors," Trans. ASME, Vol. 64, No. 1, Jan. 1942, pp. 91-104.

10. Duffie, J. A. and Beckman, W. A. "Solar Energy Thermal Processes," John Wiley and Sons, New York, 1974.

11. Ward, J. C., "Clear Sky Temperature," presented at Meeting of ISES-U.S. Section Annual Meeting, Colorado State Univ., Fort Collins, Colo., Aug. 1974

12. Souka, A. F. and Safwat, H. H., "Optimum Orientations for the Double-Exposure, Flat-Plate Collector and its Reflectors," Solar Energy, Vol. 10 No. 4, Oct.-Dec. 1966, pp. 170-174.

Table I NASA Lewis solar simulator summary

Radiation source,
243 Lamps, 300 W each
GE-type ELH, tungsten-halogen dichroic coating
12° Total divergence angle
Test area,
4 by 4 ft, maximum
Test condition limits,
Flux; 150 to 350 Btu/hr-ft^2
Flow; up to 1 gal/min (30 lb/hr-ft^2)
Inlet temp; 75° to 210° F
Wind; 0 to 10 mph at 75° F

Table II Comparison of solar simulator and air-mass 2 performance

		Air mass 2 sunlight	Simulator
Energy output percent	Ultraviolet	2.7	0.3
	Visible	44.4	48.4
	Infrared	52.9	51.3
Energy uses	Absorptivity (selective surface)	0.90	0.90
	Glass transmission	.85	.86
	Al mirror reflectivity	.86	.88
	Solar cell efficiency, percent	12.6	13.4

Table III

Collector	α_{meas} [a]	α_{cal} [b]
Black nickel collector	0.95	0.92
Black paint collector	0.95	0.93

[a] Using spectrophotometer.

[b] Calculated using experimental value of $\alpha\tau$.

Table IV Natural convection heat loss coefficients for 1 1/4 inch gap and 57° tilt angle

Approach	C		n
	T_p = 100° F	T_p = 200° F	
DeGraaf and Van Der Held	0.12	0.10	1.37
Housing and home finance	0.13	0.12	1.31
Dropkin and Somerscales	0.093	0.085	1.33
Whillier	0.18	0.18	1.25

Table V All day performance calculations
[$\theta_T = 65^\circ$; $T_{sky} = -32^\circ$ F; $T_1 = 120^\circ$ F]

Time	θ_i	Ta, $^\circ$F	K, $\alpha\tau$	K_{DR}	K_{DF}	q_T Btu/hr ft^2	η (eq. 72)	q_u $q_T \times \eta$	
Black nickel 2 glass: $a_\theta = 0.713$; $b_\theta = 0.504$; $C_\theta = 0.140$; $\overline{\alpha\tau} = 0.59$; $K_{U_L} = 1.12$									
7-8	57.4	8	---	0	1.0	2.4	-----	-----	$\eta = \frac{\Sigma q_u}{\Sigma q_T}$
8-9	43.9	7	.93	0.92	.08	106.6	-----	-----	
9-10	30.3	6	.97	.94	.06	222.5	0.354	78.7	
10-11	16.5	7	.99	.94	.06	290.8	.454	132.1	
11-12	2.8	9	1.0	.95	.05	323.9	.493	159.5	$= \frac{775.0}{1956.2}$
12-1	11.1	9	.99	.94	.06	323.8	.489	158.2	
1-2	24.8	10	.98	.95	.05	302.6	.464	140.5	$= 39.6\%$
2-3	38.5	9	.95	.93	.07	231.5	.364	84.2	
3-4	52.1	9	.90	.93	.07	152.1	.143	21.7	
Totals						1956.2		775.0	
Black 2 glass: $a_\theta = 0.728$; $b_\theta = 0.705$; $C_\theta = 0.251$; $\overline{\alpha\tau} = 0.57$; K_{UL} 1.03									
7-8	57.4	8	---	-----	1.0	2.4	-----	-----	$\eta = \frac{\Sigma q_u}{\Sigma q_T}$
8-9	43.9	7	.92	0.92	.08	106.6	-----	-----	
9-10	30.3	6	.96	.94	.06	222.5	0.253	56.3	
10-11	16.5	7	.99	.94	.06	290.8	.388	112.7	
11-12	2.8	9	1.0	.95	.05	323.9	.438	141.7	$= \frac{775.0}{1956.2}$
12-1	11.1	9	.99	.94	.06	323.8	.434	140.8	
1-2	24.8	10	.97	.95	.05	302.6	.402	121.5	$= 32.5\%$
2-3	38.5	9	.94	.93	.07	231.5	.269	62.2	
3-4	52.1	9	.98	.93	.07	152.1	-----	-----	
Totals						1956.2		635.0	

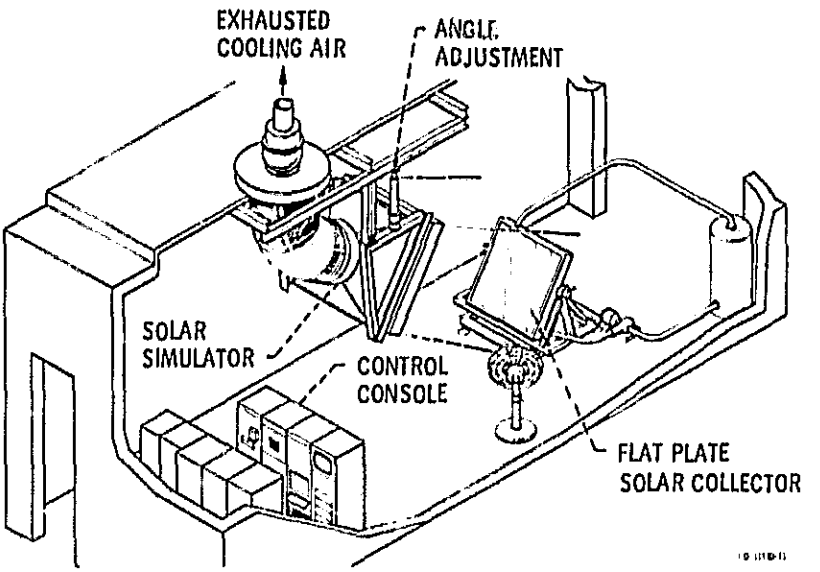

Figure 1. - Indoor test facility.

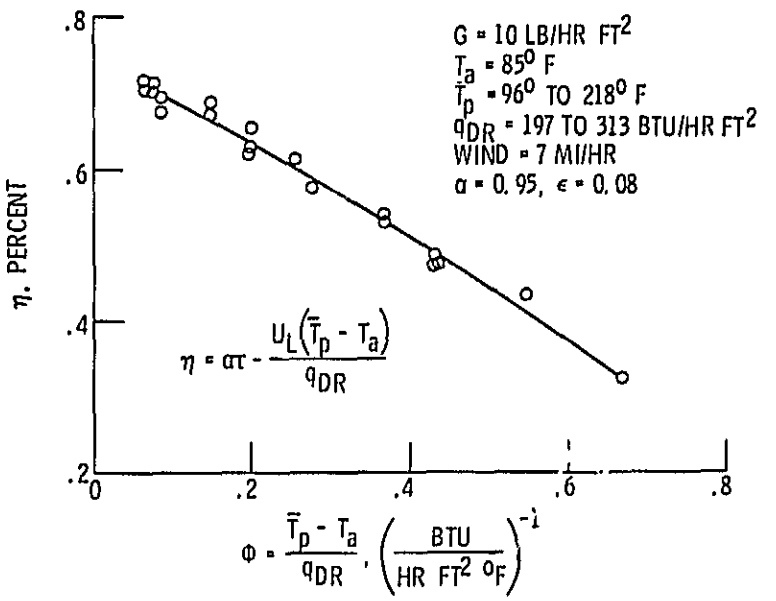

(A) HONEYWELL/LeRC BL Ni 2 GLASS.

Figure 2. - Collector performance correlation.

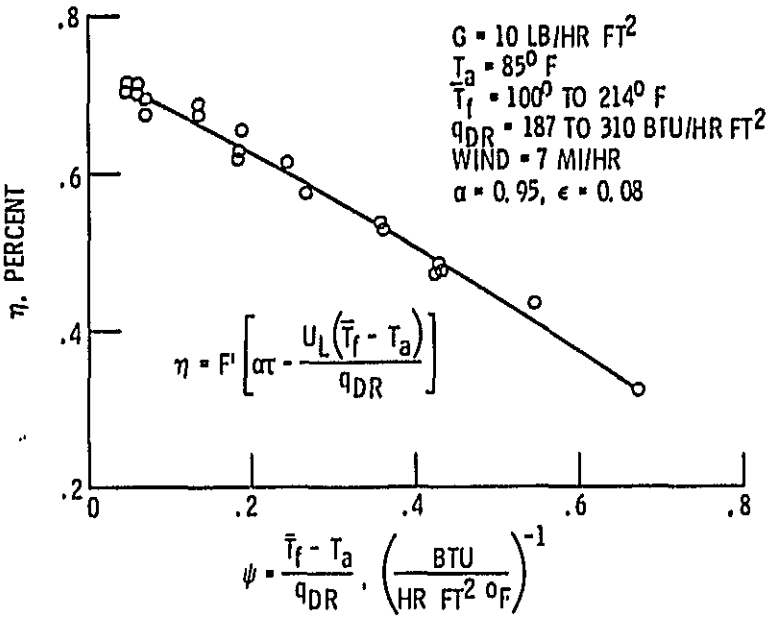

(B) HONEYWELL/LeRC BLACK Ni 2 GLASS.

Figure 2. - Continued.

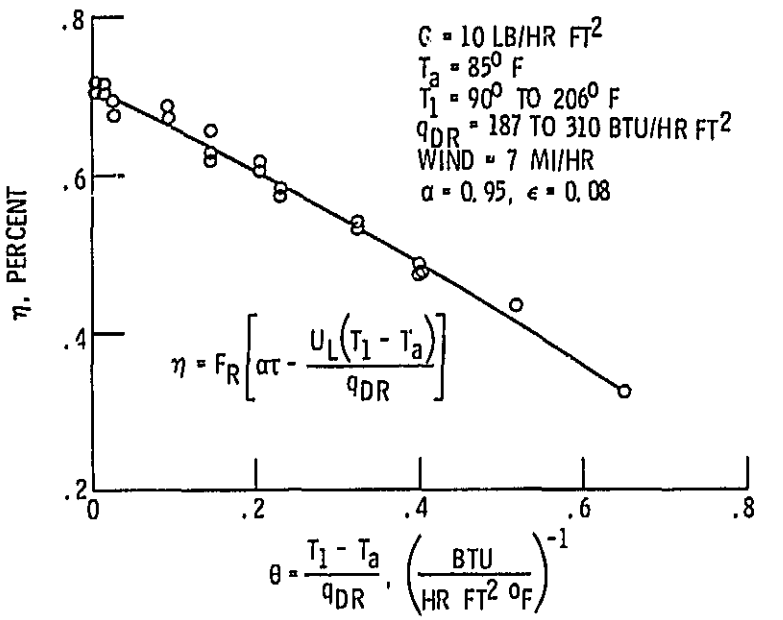

(C) HONEYWELL/LeRC BL Ni 2 GLASS.

Figure 2. - Concluded.

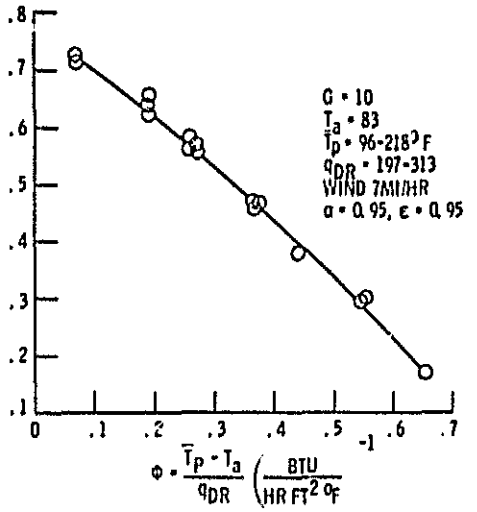

(A) HONEYWELL/LeRC BLACK PAINT 2 GLASS.

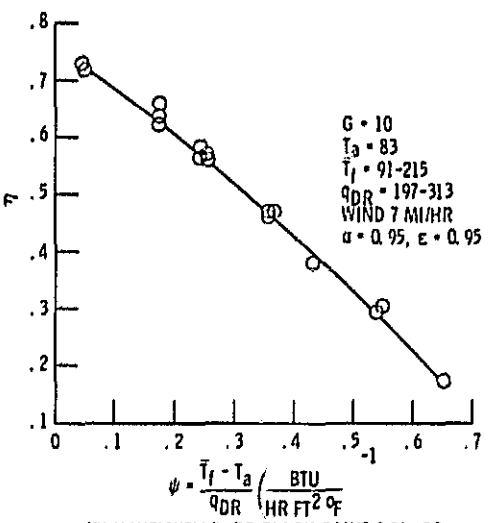

(B) HONEYWELL/LeRC BLACK PAINT 2 GLASS.

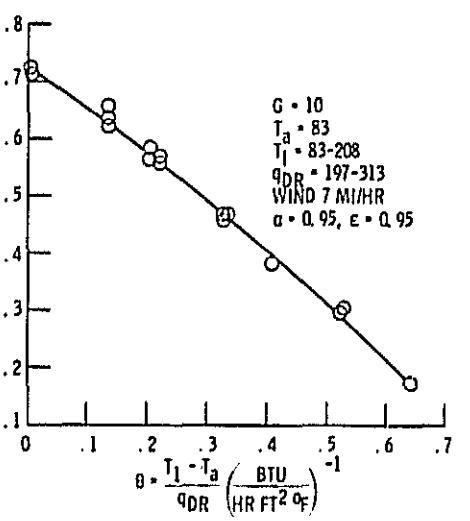

(C) HONEYWELL/LeRC BLACK PAINT 2 GLASS.

Figure 3. - Collector performance correlation.

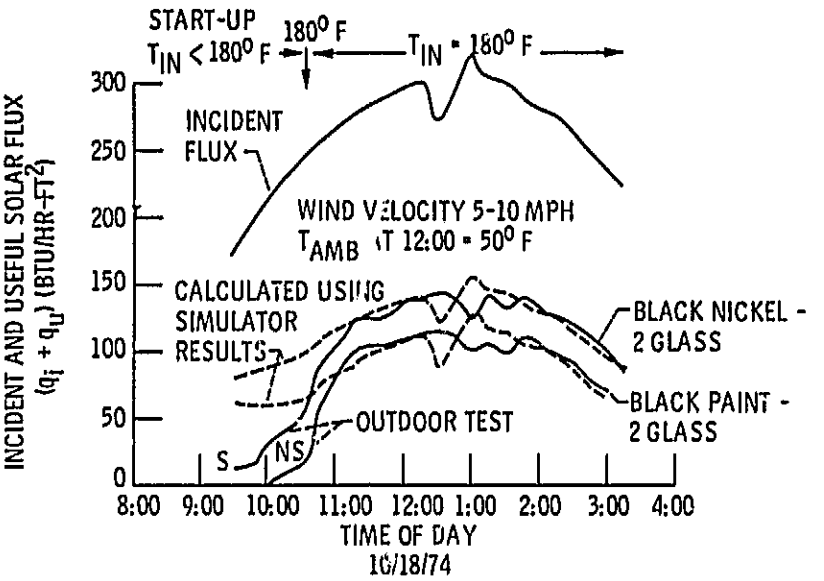

Figure 4. - Outdoor vs. indoor (simulator) collector tests.

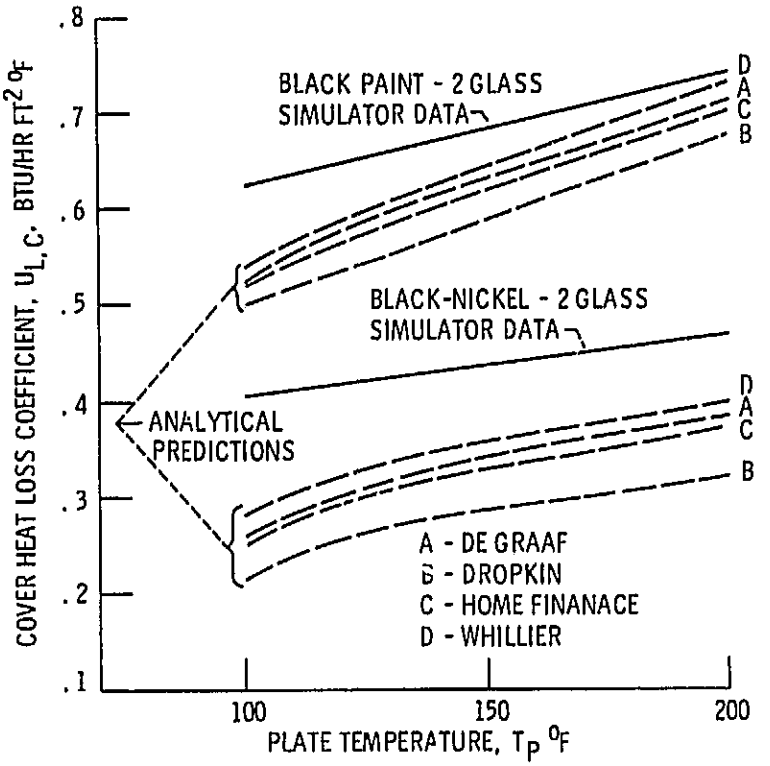

Figure 5. - Comparison of simulator results with analysis.

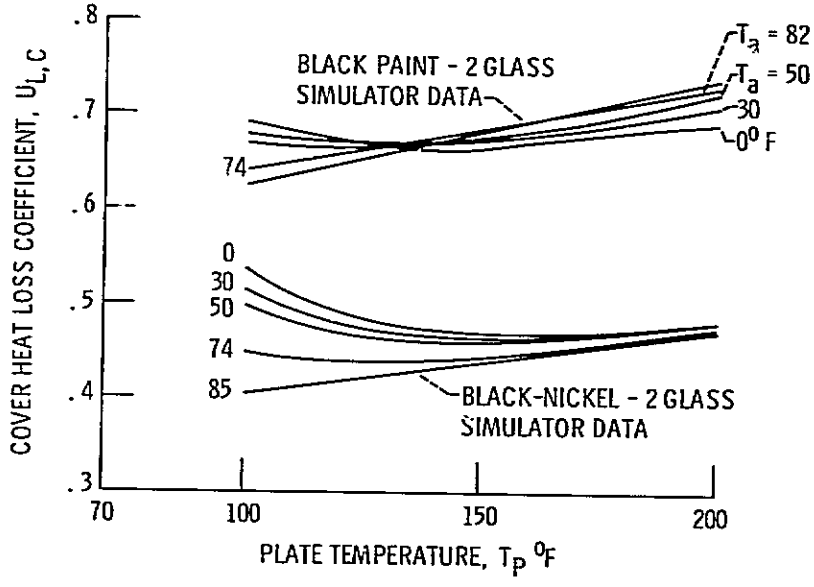

Figure 6. - Effect of ambient temperature on heat loss coefficient.

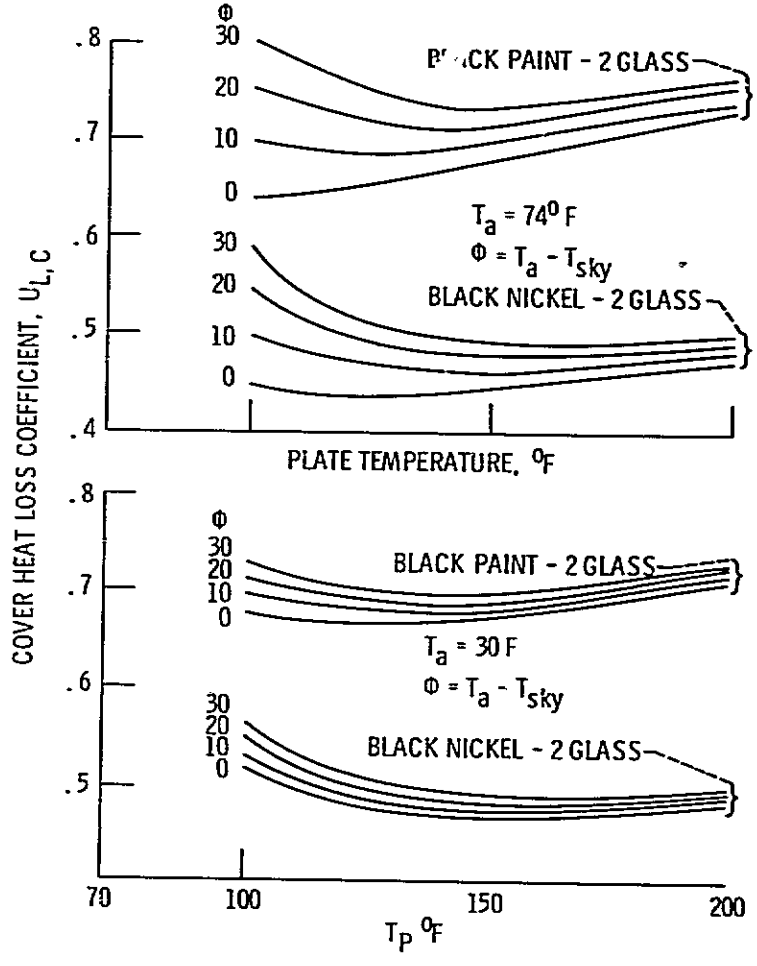

Figure 7. - Effect of sky temperature on heat loss coefficient.

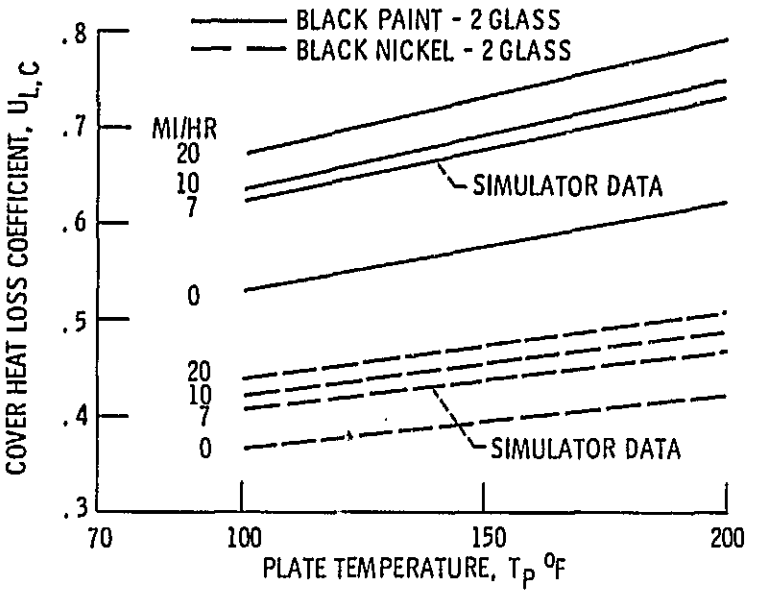

Figure 8. - Effect of wind on heat loss coefficient.

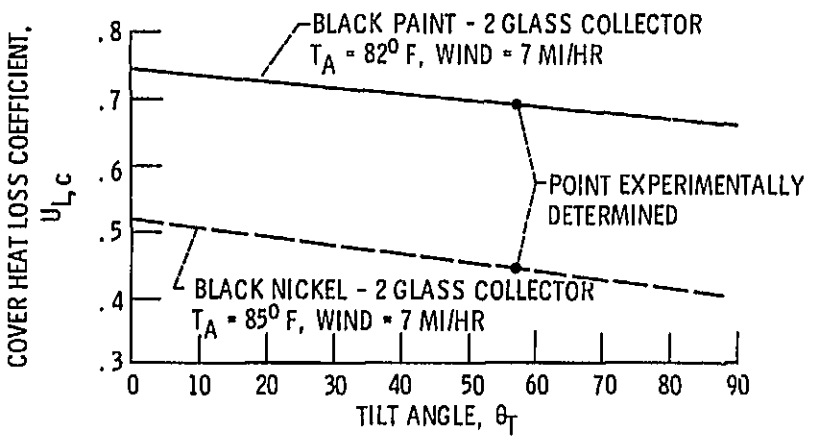

Figure 9. - Effect of tilt angle on heat loss coefficient, T_P = 160° F.

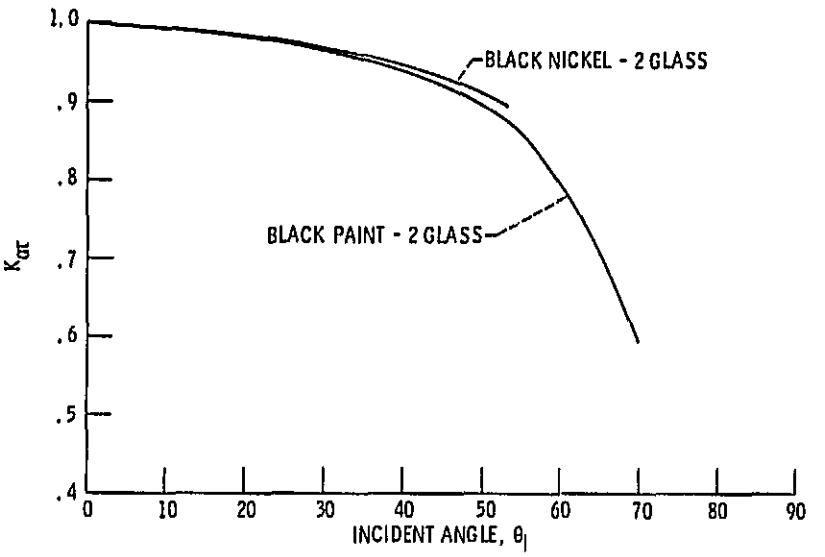

Figure 10. - Calculated incident angle modifier.

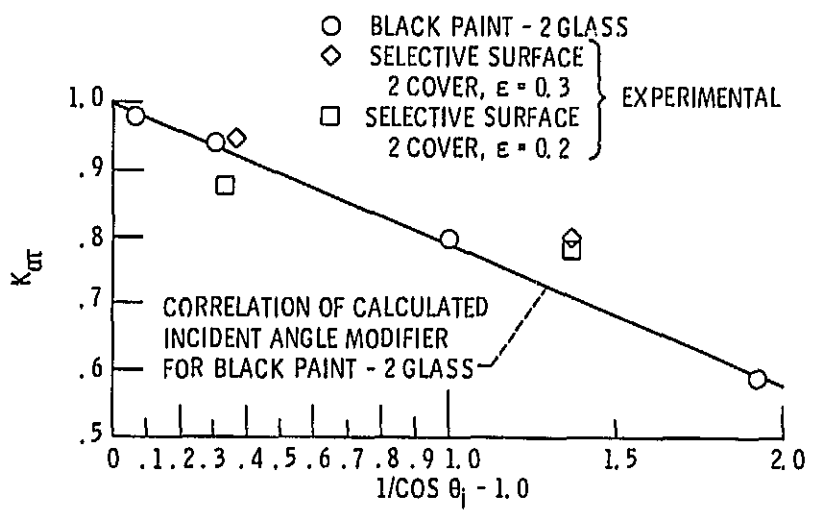

Figure 11. - Correlation of incident angle modifier.